Thin film flexible/bendable acoustic wave devices: Evolution, hybridization and decoupling of multiple acoustic wave modes

R. Tao, W.B. Wang, J.T. Luo, S. Hasan, H. Torun, P. Canyelles-Pericas, J. Zhou, W.P. Xuan, Michael Cooke, D. Gibson, Q. Wu, W.P. Ng, J.K. Luo, Y.Q. Fu

PII:	S0257-8972(18)31149-6
DOI:	doi:10.1016/j.surfcoat.2018.10.042
Reference:	SCT 23905
To appear in:	*Surface & Coatings Technology*
Received date:	21 August 2018
Revised date:	26 September 2018
Accepted date:	16 October 2018

Please cite this article as: R. Tao, W.B. Wang, J.T. Luo, S. Hasan, H. Torun, P. Canyelles-Pericas, J. Zhou, W.P. Xuan, Michael Cooke, D. Gibson, Q. Wu, W.P. Ng, J.K. Luo, Y.Q. Fu , Thin film flexible/bendable acoustic wave devices: Evolution, hybridization and decoupling of multiple acoustic wave modes. Sct (2018), doi:10.1016/j.surfcoat.2018.10.042

Thin film flexible/bendable acoustic wave devices: evolution, hybridization and decoupling of multiple acoustic wave modes

R. Tao,[1,*] W. B. Wang,[2,*] J. T. Luo,[3,!] S. Hasan,[1] H. Torun,[1] P Canyelles-Pericas,[1] J. Zhou,[4] W.P. Xuan,[5] Michael Cooke,[6] D. Gibson,[7] Q. Wu,[1] W.P. Ng,[1] J. K. Luo,[5] Y. Q. Fu,[1,!]

[1]Faculty of Engineering and Environment, Northumbria University, Newcastle upon Tyne, NE1 8ST, UK

[2] Southwest China research institute of electronic equipment, Chengdu 610036, China

[3] College of Physics and Energy, Shenzhen Key Laboratory of Sensor Technology, Shenzhen University, 518060, People's Republic of China

[4] College of Mechanical and Vehicle Engineering, Hunan University, Changsha 410082, P. R. China

[5] College of Electronics and information, Key Lab of RF Circuits and Systems, Ministry of Education, Hangzhou Dianzi University, Hangzhou 310018, P. R. China

[6] Department of Engineering, Durham University, South Road, Durham, DH1 3LE, UK

7 Institute of Thin Films, Sensors & Imaging, University of the West of Scotland, Scottish Universities Physics Alliance, Paisley PA1 2BE, UK

[8] Institute of Renewable Engineering and Environment Technology, University of Bolton, Deane Road, Bolton, BL3 5AB, UK

* These two authors have equal contribution to this paper.

!Corresponding author: Prof. Jingting Luo, luojt@szu.edu.cn; Prof. Richard Y.Q. Fu, Richard.fu@northumbria.ac.uk;

Abstract

Based on theoretical analysis, finite element simulation and experimental verifications, we have systematically investigated evolution, hybridization and decoupling of multiple acoustic wave modes and vibration patterns generated from piezoelectric film acoustic wave devices fabricated on flexible thin foils/plates. ZnO piezoelectric films deposited on flexible and bendable Al foil and plates were selected for this particular study. The ZnO/Al acoustic wave devices were chosen with wavelengths varied from 12 to 800 μm, ZnO film thickness from 2 to 10 μm and Al foil/plate thickness from 10 to 600 μm. Multiple acoustic wave modes (including symmetrical and asymmetrical Lamb waves, Rayleigh waves and higher harmonic/Sezawa wave modes) were generated, hybridized occasionally with each other, and then easily decoupled by changing the ratios of the substrate/film thicknesses to wavelengths. Ratios between device wavelength and substrate/film thickness have been identified to be the dominant parameter in determining the evolution and hybridization of multiple wave modes and their vibration patterns, which provide useful design guidance for both sensing and microfluidic applications using these flexible and bendable acoustic wave devices.

Keywords: Acoustic waves; Surface acoustic wave; Lamb wave; Flexible devices ZnO; thin films

1. Introduction

Extensive research has been performed to develop new generations of flexible, bendable, deformable and even stretchable devices in recent years, mainly motivated by increasing demand for wearable, mobile, internet-of-things, and point-of-care sensor technologies[1,2]. A variety of

flexible devices such as transistors[3], thermoelectric devices[4], batteries, solar cells[5–7], displays[8,9], and sensors[10,11] have been introduced. Currently, flexible and deformable devices are not only supplementary to the well-established rigid counterparts, but also becoming critical components for future electronics and microsystems[12].

Acoustic wave devices, especially those based on surface acoustic wave (SAW), are one of the key building blocks for modern electronics, microsensors and acoustofluidics[13–16]. These devices are generally manufactured on rigid substrates[17,18], thus they are not suitable for applications that need flexible devices. For these applications, piezoelectric thin films can be deposited onto low-cost and flexible substrates such as polymers, plastics or metallic foils/plates, which are bendable, deformable and/or recyclable[19–23]. In this case, the wavelength, λ, of acoustic wave devices is often much larger than the thickness of the substrate[24,25]. Consequently, the wave modes in these substrates may not be pure Rayleigh SAWs, but also consist of commonly observed Lamb waves when the thickness of the devices is much smaller than the designed wavelength λ, where waves cannot be confined to the region close to the top surface. These Lamb waves are normally generated on a thin plate using an external acoustic wave source or on a membrane coated with piezoelectric thin films such as PZT, ZnO and AlN[26–29].

Thin plates or membranes generally have two types of Lamb wave modes at lower frequencies[30]: antisymmetric (or flexural) mode-A mode, and symmetrical (or extensional) mode-S mode. Evolution of these modes as a function of substrate thickness has been extensively studied for the thin rigid acoustic wave devices or bulk plates[31,32]. At high frequencies, the wave velocity of

the zero-order asymmetric Lamb mode (A_0) approaches the Rayleigh wave velocity, and the wave mode gradually changes into fundamental Rayleigh wave (R_0) or higher order mode wave with decreasing wavelength. Similarly, at high frequencies, the S mode also converges towards the Rayleigh wave mode[31,32].

Polymers and metal foils have recently been explored to fabricate flexible acoustic wave devices for sensing, microfluidics and lab-on-chip applications[33–36]. Although most flexible acoustic wave devices are fabricated onto polymers, there are significant challenges to attain good performance due to certain limitations: (1) significant attenuation/dissipation of acoustic wave energies into polymer substrates; (2) significant mismatch between crystal structures and thermal expansion coefficients of the polymer substrates and the piezoelectric films, which will induce large film stress and result in poor adhesion.

These limitations of polymeric substrates can be mitigated using flexible metallic foils. For example, Al foils promote texture growth of ZnO films, provide good film adhesion, and keep film stress under control during deposition, and most importantly, significantly reduce the propagation loss of the waves[37]. Furthermore, compared with their polymer counterparts, Al foils have distinct advantages of deformability (forming and then maintaining temporary shapes) and re-deformability, which solve many common problems associated with most polymer-based flexible devices (for example, large energy dissipation and permanent original or deformed shapes). Using commercially available large area Al foils, thin film deposition processes, and mass-production methods such as roll-to-roll processing and printing, high performance

flexible/deformable acoustic wave sensors and microfluidic devices can be realized at a low cost[38].

Recently, we have successfully demonstrated flexible ultrasonic and acoustic wave devices on commercially available 50 μm-thick Al foils with ZnO layers for microfluidic applications[39,40]. Initial results confirmed the presence of dual mode waves or multiple mode waves of both Lamb and Rayleigh waves in the devices. It is known that hybridized waves could result in efficient liquid actuation, but hybridization may pose complications for sensing application as decoupling of these wave modes through change of wavelengths or film/substrate thicknesses is essential to track a specific wave mode and a resonant peak. For example, Zhou et al[41] revealed that the A_0 mode is more sensitive to density changes, while the S_0 mode is more sensitive to viscosity changes in Lamb wave devices. The reason is that the wave mode with an out-of-plane motion (longitudinal wave dominant) is sensitive to density changes, whereas the wave mode with an in-plane motion (shear wave or transverse wave) is more sensitive to viscosity. Therefore, these two modes can be used selectively for density and viscosity sensing. He et al. also reported this decoupling effect for the bendable ZnO thin film SAW on PET[42].

Lamb wave propagation on a stand-alone metal plate has been well documented.[43] However, so far, the literature lacks a systematic study on evolution, hybridization and decoupling of these waves (including Rayleigh mode based SAWs, Sezawa mode SAWs, A mode and S mode of Lamb waves, as well as higher harmonic modes of Lamb or Rayleigh waves) in the acoustic wave devices, in particular ZnO film-deposited devices realized onto flexible metallic foil substrates. In

this paper, we report theoretical and experimental studies of the evolution, hybridization and decoupling of wave modes in the flexible acoustic wave devices to provide a design guideline for different sensing and microfluidic applications.

2. Theoretical, numerical modeling and experimental details

2.1. Theoretical analysis and numerical modeling

A theoretical analysis was reported using a two-layer model to investigate acoustic wave modes in a ZnO/foil system[44–46]. The ZnO thin film have *c*-orientation with in-plane isotropic and ideal material properties. XRD measurement result of the ZnO film on Al substrate is shown in Fig. SI1 in the supporting information). No shear horizontal wave was considered. The acoustic wave in the two layers can be described using the following equations:

$$c_{ijkl}^{[r]} u_{kli}^{[r]} + e_{kil}^{[r]} \phi_{ik}^{[r]} = \rho^{[r]} u_j^{[r]} \quad (1)$$

$$e_{ijk}^{[r]} u_{k,ki}^{[r]} - \varepsilon_{ij}^{[r]} \phi_{ij}^{[r]} = 0 \quad (2)$$

where $c_{ijkl}^{[r]}$, $e_{kij}^{[r]}$ and $\varepsilon_{ij}^{[r]}$ are the elastic, piezoelectric and dielectric constants; $\rho^{[r]}$ the density, and $u_{kli}^{[r]}$, $\phi_{ik}^{[r]}$ represent particle displacements and potentials in the *k* direction, respectively. The superscript *r*=1, 2 denotes the layer number for the ZnO thin film and the Al substrate, respectively.

Finite element analysis (FEA) of the ZnO/Al foil double layer structure to obtain vibration patterns was performed using COMSOL software. A simplified 2-dimensional (2D) model with ideal material parameters, one pair of interdigital transducers (IDTs) electrode and infinite

boundary conditions were used to simulate SAW devices with different wavelengths. SAW device models were defined using the piezoelectric equation as follows[47,48]:

$$T_{ij} = c^{E}_{ijkl} S_{kl} - e^{t}_{ijk} E_k \tag{3}$$

$$D_i = e_{ikl} S_{kl} - \varepsilon^{s}_{ij} E_j \tag{4}$$

where $\boldsymbol{T}$ is the stress vector, $\boldsymbol{D}$ the electrical displacement (C/m^2), c^E the elasticity matrix (N/m^2), $\boldsymbol{e}$ the piezoelectric matrix (C/m^2), $\boldsymbol{E}$ the electric field vector (V/m), ε^s the permittivity matrix (F/m) and $\boldsymbol{S}$ the strain vector. The superscripts *E* and *S* represent the constant electric field and stress condition, respectively. After solving the Newton and Maxwell equations related to equations 2 and 3, the relationship between global displacement *u* and potential voltage *V* can be obtained[47]:

$$\sum_{ijk} C^{E}_{ijkl} \frac{\partial^2 u_l}{\partial x_j \partial x_k} + \sum_{jk} e_{kij} \frac{\partial^2 V}{\partial x_j \partial x_k} = \rho \frac{\partial^2 u_i}{\partial t^2} \tag{5}$$

$$\sum_{kl} e_{jkl} \frac{\partial^2 u_l}{\partial x_j \partial x_k} - \sum_{jk} \varepsilon^{s}_{jk} \frac{\partial^2 V}{\partial x_j \partial x_k} = 0 \tag{6}$$

where *i*, *j*, *k*, *l* = 1, 2 and 3.

For theoretical analysis and FEA simulation, the thickness of the ZnO film was set to be 2, 5, 7 and 10 μm, and the thicknesses of the Al foil/plates were varied from 10 to 600 μm, respectively. The wavelength was varied from 12 to 800 μm. A polarization voltage of 1 V was assigned to the electrode. ZnO thin film layer was considered as planar or in-plane isotropic during the simulations. The material parameters, consistent with the values in the literature[47], are listed in Table 1. Since the thin film devices were mostly operating in plate modes, all the boundaries were set to be free. The structure was meshed in triangular modes. For the devices with different

wavelengths, the numbers of mesh elements were varied with a minimum number of 10,000, and the maximum element units were varied from 0.1 to 2 μm depending on the wavelength.

Table 1. The parameters used for the theoretical analysis

Material	Thickness h (μm)	Young's modulus E (GPa)	Poisson's ratio υ	Piezoelectric constant (c/m^2) e	Relative dielectric constant ε	Density ρ (kg/m^3)
ZnO	2, 5, 7, 10	120	0.446	1.32	10.2	5610
Al	10, 50, 100, 200, 500, 600	69	0.33	-	-	2700

2.2 Microfabrication of Devices

We fabricated and experimentally characterized flexible acoustic waves to compare with our simulations. ZnO thin films with various thicknesses from 2 to 10 μm were deposited on Al foils (with thicknesses of 50, 200 and 600 μm) using a direct current (DC) magnetron sputter system (NS3750, Nordiko). A 99.99% pure zinc target was sputtered at a power of 400 W. The chamber pressure during deposition was set at ~0.65 Pa with an Ar/O_2 gas flow rate of 3/10 sccm. The distance between the target and substrate was 20 mm, and the substrates were rotated during deposition without intentional substrate heating. Acoustic wave devices with IDTs were fabricated using conventional photolithography and lift-off processes. The thickness of the electron beam

evaporated Cr/Au electrodes was 20/100 nm. The SAW resonators had 30 pairs of IDT fingers with an aperture of 4.9 mm. The wavelength of the devices was varied from 20 to 800 μm. The reflection (S_{11}) spectra of the acoustic wave devices were measured using a vector network analyzer (Agilent E5061B) (See Fig. SI2(a) and (b)).

3. Results and discussions

3.1. Evolution, hybridization and decoupling of wave modes

The resonant frequencies as a function of the wavelength of ZnO on Al foil (50 μm) SAW devices are shown in Fig. 1 based on the theoretical calculations using the FEA two-layer model[44–46]. In addition, the measured values of the resonant frequencies for various devices with different wavelengths are shown in Fig. 1 for comparison. The calculated resonant frequencies for typical acoustic wave modes, i.e., A_0, S_0, and R_0 show reasonable agreements with our measured data. However, when the wavelength is larger than 100 μm, there are discrepancies between the theoretical results and the measured ones. These discrepancies can be attributed to combined effects, including nonuniformity in the thickness of the deposited films, scattering at the interface between the piezoelectric layer and Al foil substrate, deviations between material constants used in theoretical analysis and those of the fabricated polycrystalline films, and the simplified FEA model using one pair of IDT fingers and infinite boundary conditions.

FEA simulations provide extensive information about the wave vibration patterns of the flexible devices. Fig. 2 shows the results of FEA simulations for ZnO (5μm)/Al (50μm) bi-layer, including vibration patterns and resonant frequencies as functions of both wavelength and vibration mode.

The Rayleigh vibration modes and 1st Sezawa modes can be clearly observed when the wavelength is equal and smaller than 40 μm. Whereas the Lamb wave modes of both A and S modes are dominant when the wavelength is above 40 μm. Our results in Fig. 2 show that there is hybridized mode of Rayleigh R0 and Lamb A0 modes when the wavelength is about 64 μm (frequency of 40.96 MHz).

In order to verify at what frequency range these two modes are hybridized together, we have further performed FEA simulations of wave modes for the devices with various wavelengths from 45 μm to 60 μm with the Al and ZnO thicknesses fixed at 50 μm and 5 μm, respectively. The obtained results shown in Fig. 3(a) clearly indicate that hybridized modes of Rayleigh R0 and Lamb A0 modes occur at a wide range of wavelengths, e.g., from about 44 μm up to about 72 μm, and the vibration modes are slightly different at different frequencies. We define these modes as the pseudo-R0 mode and pseudo-A0 mode. It also means that there are slight shape changes of the vibration patterns and gradual evolutions from Lamb waves into Rayleigh with the decrease of wavelengths. We have calculated the ratio between the surface vibrations amplitudes and the backside vibration amplitudes and draw the data as a function of wavelength between 32 μm to 100 μm, and the data are shown in Fig. 3(b). Clearly there is a wide range of wavelengths where the hybridization of two waves exists. From Fig. 2, for the wavelength of 100 μm, there is also a hybridized mode of pseudo-Sezawa mode and pseudo-A1 Lamb wave overlapping at a frequency of 51.96 MHz.

Since wave modes are influenced by the thicknesses of both the piezoelectric layer and the

substrate, it is reasonable to characterize them using the ratio of wavelength to the total thickness (λ/H, H being the combined thickness of ZnO/Al). For the results discussed in this section, the total thickness of the ZnO (5μm)/Al (50μm) structure is fixed at 55 μm whereas the wavelength is varied. When the wavelength is large ($\lambda/H \geq 2$), flexural types of Lamb waves are dominant, propagating through the whole Al foil. When the wavelength becomes smaller ($\lambda/H <= 1$), Rayleigh mode (R_0) and Sezawa modes emerges. When the wavelength is 64 μm, R_0 and A_0 exhibit at the same vibration pattern with the same resonant frequency. With further decrease in wavelength ($\lambda/H << 1$), Rayleigh mode gradually becomes dominant, emerging as the first resonant peak, and followed with the Sezawa mode (including 1^{st} and 2^{nd} harmonic, etc.).

Fig. 4 shows the measured resonant frequencies of the S_{11} spectrum for the devices with wavelengths varied from 20 to 800 μm. Multiple wave modes with different frequencies are clearly observed, which is very common in SAW and Lamb wave devices. Based on the calculation and vibration patterns of the simulation results, we can precisely identify multiple wave modes as R_0, A_0, S_0, A_1, S_1 and Sezawa modes. The measured frequencies of all the wave modes decrease with increasing wavelength. A larger wavelength (or larger λ/H value) means a larger percentage of wave propagation is confined in the Al foil as shown in Fig. 4(a), and Lamb waves are dominant. Whereas, for the samples with wavelength smaller than the substrate thickness of 50 μm, the Rayleigh and Sezawa modes are dominant as shown in Fig. 4(b). The measured frequency depends on the wavelength for all the devices with various modes as shown in Fig. 4(c), together with those from the simulation for comparisons. The simulated and measured data show reasonably good agreements. It is possible to decouple the overlapped wave modes by

modifying the ratio, e.g., simply by changing the wavelength or film/foil thickness.

3.2. Generation and evolution of wave modes with ZnO film thickness

In this section, we will focus on the effect of ZnO film thickness on the characteristics of ZnO/Al devices. We simulated the devices on a 50-μm thick Al foil with ZnO film thickness varied from 2 to 10 μm. The simulation results are shown in Fig. 5. Devices with wavelength of 400, 64, and 12 μm were selected for discussion as they represent three typical conditions of λ/H >>1, ~1 and <<1, respectively. The Rayleigh and Sezawa waves become dominant for the devices with a wavelength of 12 μm, which is much smaller than the foil thickness, as shown in Fig. 5(a). When the wavelength is increased to 64 μm (Fig. 5b), it becomes comparable to the plate thickness (λ/H~1), thus leading to hybridized Rayleigh and A_0 modes. Both the resonant frequency and phase velocity decrease slightly with increasing ZnO thickness since the velocity in ZnO is slightly smaller than that in Al[39]. On the other hand, as shown in Fig. 5c, only Lamb wave modes are dominant for the devices with a wavelength of 400 μm (λ/H>>1). The resonant frequencies and phase velocities for these devices are almost constants, indicating the effect of ZnO film thickness is negligible. To sum up, there are no significant changes in the frequencies and velocities as a function of ZnO film thickness, especially for the devices with larger wavelengths.

3.3. Wave modes with varied thickness of Al foil/plate

We further investigated the resonant frequencies and wave modes with various Al foil/thin plates thicknesses (from 10 to 600 μm) with a fixed ZnO film thickness of 5 μm. Fig. 6 shows the results of the simulated resonant frequencies of A_0, S_0 and A_1, S_1 and R_0 as a function of Al foil thickness.

The Rayleigh mode is again dominant when the wavelength is 12 μm, when the foil and plates are thicker than 10 μm and above as shown in Fig. 6(a). Fig. 6(b) shows Rayleigh waves are still dominant with increasing Al foil thickness when the wavelength is not too large as compared with the device thickness ($\lambda/H \leq 1$), whereas flexural Lamb waves are apparently dominant when the Al foil thickness is below 50 μm. The phase velocities of different modes converge to a fixed value with increasing Al thickness. When the wavelength is 400 μm, the Rayleigh mode is not observed, and the frequency depends on the Al thickness similar to the Lamb wave of the single-layered plate structure.

Fig. 7(a) shows simulated vibration modes of ZnO/Al SAW devices with Al thickness of 200 μm and Fig. 7(b) shows the corresponding measured multiple wave modes. The Lamb wave vibration mode is clearly observed in the SAW devices with wavelengths of 300 to 400 μm. A_0 and pseudo-R0 modes of the devices are hybridized together at 13.80 MHz with a wavelength of 200 μm. There is another hybridized mode of pseudo-Sezawa and A1 modes at a frequency of 18.72 MHz. Whereas when the wavelength is smaller than 100 μm, there are only Rayleigh and Sezawa modes observed, without apparent Lamb waves.

We then fabricated acoustic wave devices using Al plates with thickness of 200 μm with different wavelengths to validate our simulations. The measured wave modes match well with the simulated ones and the devices show a mixture of Rayleigh, Lamb waves, Sezawa wave, and higher harmonic wave modes. Based on the calculation and simulation results, we can precisely identify the measured multiple wave modes with R_0, A_0, S_0, A_1, S_1, A_2, S_2, and Sezawa wave. These

devices have various wave modes and it can be used for various sensing applications by choosing different wave modes. Fig. 7(c) shows the simulated and measured frequency of different types of wave modes as a function of wavelength in a log-log scale. Clearly, the measured frequencies are in good agreement with the simulated ones and the frequency of all the wave modes decreases linearly with increasing wavelength.

Fig. 8(a) shows simulated vibration modes of ZnO (5 μm)/Al (600 μm) acoustic wave devices and Fig. 8(b) shows the corresponding experimentally measured multiple wave modes. It can be observed from Fig. 8(a) that Rayleigh and Sezawa modes appear in the devices with the wavelengths of 100 and 200 μm. However, A0 Lamb waves were found to be hybridized with the pseudo-Rayleigh R0 mode for the devices with wavelengths of 300 and 400 μm. Simultaneously at these two wavelengths, Sezawa mode waves are also obtained. We have verified these simulation results based on our experimental results as we clearly labeled the observed modes in Fig. 8(b).

4. Conclusions

We have analyzed, simulated, fabricated and characterized flexible and bendable ZnO/Al foil acoustic wave devices with varied wavelengths (from 10 to 800 μm), varied ZnO film thickness (from 2 to 10 μm) and varied Al layer thickness (from 10 to 600 μm). We have observed and explained the generation and evolution of multiple acoustic wave modes (including symmetrical and asymmetrical Lamb waves, Rayleigh waves, Sezawa modes, and higher harmonic wave modes) based on theoretical and simulation results. We have validated our simulations with

experimental data. Our findings show that the key factor for the generation and evolution of multiple acoustic wave modes is λ/H ratio. When the ratio λ/H <<1, Rayleigh wave would be dominant for the fundamental wave mode. Sezewa and some other higher harmonic wave modes may also exist. When the ratio λ/H >>1, the propagating waves would be Lamb wave modes. Thickness of ZnO layer has some effect on Rayleigh mode but not significant to the Lamb mode, especially for large wavelengths. Most of devices have many hybrid modes, but the wave modes can be decoupled by changing the film/foil thicknesses. Decoupling the wave modes and simultaneously measuring the individual frequencies allow multi-parameter sensing, such as mass loading, viscosity, or conductivity changes. These multiple-mode flexible acoustic wave devices are structurally simple, more accurate in detection, and can be fabricated at a low cost, and hence are promising for applications in flexible sensors and electronics.

Acknowledgments: Funding support from the UK Engineering and Physical Sciences Research Council (EPSRC) for support under grant EP/P018998/1 Newton Mobility Grant (IE161019) through Royal Society and the National Natural Science Foundation of China, and Royal academy of Engineering UK-Research Exchange with China and India, NSFC (51302173, 61274037), National Key Research and Development Program of China (Grant no. 2016YFB0402705), Foundation for Distinguished Young Talents in Higher Education of Guangdong (Grant no. 2013LYM_0078), Basical Research Program of Shenzhen (Grant no. JCYJ20140418091413493). Wenbo Wang acknowledges the Lin Guangzhao & Hu Guozan Graduate Education International Exchange Fund for sponsoring his study in UK. Following persons are acknowledged for participating the work during the studies: Mr. Andrew Bunyan, Dr. Yifan Li, Dr. Chao Zhao, Dr.

Yong Liu, Ahmed El-Hady, and Dr. Xingli He.

References:

[1] Rogers J A, Someya T and Huang Y 2010 Materials and mechanics for stretchable electronics. *Science* **327** 1603–7

[2] Kim D-H, Ghaffari R, Lu N and Rogers J A 2012 Flexible and Stretchable Electronics for Biointegrated Devices *Annu. Rev. Biomed. Eng.* **14** 113–28

[3] Georgiou T, Jalil R, Belle B D, Britnell L, Gorbachev R V., Morozov S V., Kim Y J, Gholinia A, Haigh S J, Makarovsky O, Eaves L, Ponomarenko L A, Geim A K, Novoselov K S and Mishchenko A 2013 Vertical field-effect transistor based on graphene-WS 2 heterostructures for flexible and transparent electronics *Nat. Nanotechnol.* **8** 100–3

[4] Fan P, Zheng Z H, Li Y Z, Lin Q Y, Luo J T, Liang G X, Cai X M, Zhang D P and Ye F 2015 Low-cost flexible thin film thermoelectric generator on zinc based thermoelectric materials *Appl. Phys. Lett.* **106** 73901

[5] Kim B J, Kim D H, Lee Y Y, Shin H W, Han G S, Hong J S, Mahmood K, Ahn T K, Joo Y C, Hong K S, Park N G, Lee S and Jung H S 2015 Highly efficient and bending durable perovskite solar cells: Toward a wearable power source *Energy Environ. Sci.* **8** 916–21

[6] Beaujuge P M and Fréchet J M J 2011 Molecular Design and Ordering Effects in π-Functional Materials for Transistor and Solar Cell Applications *J. Am. Chem. Soc.* **133** 20009–29

[7] He Z, Xiao B, Liu F, Wu H, Yang Y, Xiao S, Wang C, Russell T P and Cao Y 2015 Single-junction polymer solar cells with high efficiency and photovoltage *Nat. Photonics* **9** 174–9

[8] Moon H C, Lodge T P and Frisbie C D 2014 Solution-processable electrochemiluminescent ion gels for flexible, low-voltage, emissive displays on plastic *J. Am. Chem. Soc.* **136** 3705–12

[9] Yin S N, Wang C F, Yu Z Y, Wang J, Liu S S and Chen S 2011 Versatile bifunctional magnetic-fluorescent responsive Janus supraballs towards the flexible bead display *Adv. Mater.* **23** 2915–9

[10] Wang Y, Yang R, Shi Z, Zhang L, Shi D, Wang E and Zhang G 2011 Super-elastic graphene ripples for flexible strain sensors *ACS Nano* **5** 3645–50

[11] Pang C, Lee G Y, Kim T Il, Kim S M, Kim H N, Ahn S H and Suh K Y 2012 A flexible and highly sensitive strain-gauge sensor using reversible interlocking of nanofibres *Nat. Mater.* **11** 795–801

[12] Nguyen N-T 2015 Research Highlight Soft Microsystems - A Paradigm Shift in Engineering Small Systems *Micro Nanosyst.* **7** 2–3

[13] Ding X, Li P, Lin S-C S, Stratton Z S, Nama N, Guo F, Slotcavage D, Mao X, Shi J, Costanzo F and Huang T J 2013 Surface acoustic wave microfluidics *Lab Chip* **13** 3626

[14] Yeo L Y and Friend J R 2014 Surface Acoustic Wave Microfluidics *Annu. Rev. Fluid Mech.* **46** 379–406

[15] Luo J, Luo P, Xie M, Du K, Zhao B, Pan F, Fan P, Zeng F, Zhang D, Zheng Z and Liang G 2013 A new type of glucose biosensor based on surface acoustic wave resonator using Mn-doped ZnO multilayer structure *Biosens. Bioelectron.* **49** 512–8

[16] Luo J T, Pan F, Fan P, Zeng F, Zhang D P, Zheng Z H and Liang G X 2012 Cost-effective and high frequency surface acoustic wave filters on ZnO:Fe/Si for low-loss and wideband

application *Appl. Phys. Lett.* **101** 172909

[17] Du X Y, Swanwick M E, Fu Y Q, Luo J K, Flewitt A J, Lee D S, Maeng S and Milne W I 2009 Surface acoustic wave induced streaming and pumping in 128° Y-cut LiNbO3for microfluidic applications *J. Micromechanics Microengineering* **19** 35016

[18] Zhou J, Demiguel-Ramos M, Garcia-Gancedo L, Iborra E, Olivares J, Jin H, Luo J K, Elhady A S, Dong S R, Wang D M and Fu Y Q 2014 Characterisation of aluminium nitride films and surface acoustic wave devices for microfluidic applications *Sensors Actuators, B Chem.* **202** 984–92

[19] Jin H, Zhou J, He X, Wang W, Guo H, Dong S, Wang D, Xu Y, Geng J, Luo J K and Milne W I 2013 Flexible surface acoustic wave resonators built on disposable plastic film for electronics and lab-on-a-chip applications *Sci. Rep.* **3** 2140

[20] He X, Guo H, Chen J, Wang W, Xuan W, Xu Y and Luo J 2014 Bendable ZnO thin film surface acoustic wave devices on polyethylene terephthalate substrate *Appl. Phys. Lett.* **104** 213504

[21] Bian X, Jin H, Wang X, Dong S, Chen G, Luo J K, Deen M J and Qi B 2015 UV sensing using film bulk acoustic resonators based on Au/n-ZnO/piezoelectric-ZnO/Al structure *Sci. Rep.* **5** 9123

[22] Fu Y Q, Luo J K, Nguyen N T, Walton A J, Flewitt A J, Zu X ., Li Y, McHale G, Matthews A, Iborra E, Du H and Milne W I 2017 Advances in piezoelectric thin films for acoustic biosensors, acoustofluidics and lab-on-chip applications *Prog. Mater. Sci.* **89** 31–91

[23] Fu Y Q, Luo J K, Du X Y, Flewitt A J, Li Y, Markx G H, Walton A J and Milne W I 2010

Recent developments on ZnO films for acoustic wave based bio-sensing and microfluidic applications: a review *Sensors Actuators B Chem.* **143** 606–19

[24] Lamb H 1917 On Waves in an Elastic Plate *Proc. R. Soc. A Math. Phys. Eng. Sci.* **93** 114–28

[25] Muralt P, Ledermann N, Paborowski J, Barzegar A, Gentil S, Belgacem B, Petitgrand S, Bosseboeuf A and Setter N 2005 Piezoelectric micromachined ultrasonic transducers based on PZT thin films *IEEE Trans. Ultrason. Ferroelectr. Freq. Control* **52** 2276–88

[26] Laurent T, Bastien F O, Pommier J C, Cachard A, Remiens D and Cattan E 2000 Lamb wave and plate mode in ZnO/silicon and AIN/silicon membrane application to sensors able to operate in contact with liquid *Sensors Actuators, A Phys.* **87** 26–37

[27] Nguyen N T and White R M 1999 Design and optimization of an ultrasonic flexural plate wave micropump using numerical simulation *Sensors Actuators, A Phys.* **77** 229–36

[28] Meng A H, Nguyen N T and WHITE R M 2000 Focused flow micropump using ultrasonic flexural plate waves *Biomed. Microdevices* **2** 169–74

[29] Nguyen N T, Meng A H, Black J and White R M 2000 Integrated flow sensor for in situ measurement and control of acoustic streaming in flexural plate wave micropumps *Sensors Actuators, A Phys.* **79** 115–21

[30] Grate J W, Wenzel S W and White R M 1991 *(28) Instruction Manual, Nitrogen Oxide Electrode* vol 63(Pergamon Press)

[31] Moroney R M, White R M and Howe R T 1991 Microtransport induced by ultrasonic Lamb waves *Appl. Phys. Lett.* **59** 774–6

[32] White R M and Wenzel S W 1988 Fluid loading of a Lamb-wave sensor *Appl. Phys. Lett.*

52 1653–5

[33] Akin N, Sebnem Cetin S, Cakmak M, Memmedli T and Ozcelik S 2013 Effect of film thickness on properties of aluminum doped zinc oxide thin films deposition on polymer substrate *J. Mater. Sci. Mater. Electron.* **24** 5091–6

[34] Prepelita P, Medianu R, Sbarcea B, Garoi F and Filipescu M 2010 The influence of using different substrates on the structural and optical characteristics of ZnO thin films *Appl. Surf. Sci.* **256** 1807–11

[35] Sierros K A, Banerjee D A, Morris N J, Cairns D R, Kortidis I and Kiriakidis G 2010 Mechanical properties of ZnO thin films deposited on polyester substrates used in flexible device applications *Thin Solid Films* **519** 325–30

[36] Min H S, Yang M K and Lee J-K 2009 Improved optical and electrical properties of rf sputtered Al doped ZnO films on polymer substrates by low-damage processes *J. Vac. Sci. Technol. A Vacuum, Surfaces, Film.* **27** 352–5

[37] Tao R, Hasan S A, Wang H Z, Zhou J, Luo J T, McHale G, Gibson D, Canyelles-Pericas P, Cooke M D, Wood D, Liu Y, Wu Q, Ng W P, Franke T and Fu Y Q 2018 Bimorph material/structure designs for high sensitivity flexible surface acoustic wave temperature sensors *Sci. Rep.* **8** 9052

[38] Zhou X S, Zhao C, Hou R, Zhang J, Kirk K J, Hutson D, Guo Y J, Hu P A, Peng S M, Zu X T and Fu Y Q 2014 Sputtered ZnO film on aluminium foils for flexible ultrasonic transducers *Ultrasonics* vol 54(Elsevier)pp 1991–8

[39] Liu Y, Li Y, El-Hady A M, Zhao C, Du J F, Liu Y and Fu Y Q 2015 Flexible and bendable acoustofluidics based on ZnO film coated aluminium foil *Sensors Actuators, B*

Chem. **221** 230–5

[40] Liu Y, Luo J T, Zhao C, Zhou J, Hasan S A, Li Y, Cooke M, Wu Q, Ng W P, Du J F, Yu Q, Liu Y and Fu Y Q 2016 Annealing Effect on Structural, Functional, and Device Properties of Flexible ZnO Acoustic Wave Sensors Based on Commercially Available Al Foil *IEEE Trans. Electron Devices* **63** 4535–41

[41] Zhou L, Wu Y, Xuan M, Manceau J F and Bastien F 2012 A multi-parameter decoupling method with a Lamb wave sensor for improving the selectivity of label-free liquid detection *Sensors (Switzerland)* **12** 10369–80

[42] He X L, Zhou J, Wang W B, Xuan W P, Yang X, Jin H and Luo J K 2014 High performance dual-wave mode flexible surface acoustic wave resonators for UV light sensing *J. Micromechanics Microengineering* **24** 55014

[43] Wang T, Mu X, Kropelnicki P, Randles A B and Lee C 2014 Viscosity and density decoupling method using a higher order Lamb wave sensor *J. Micromechanics Microengineering* **24** 75002

[44] Chen Z, Fan L, Zhang S and Zhang H 2014 Theoretical research on ultrasonic sensors based on high-order Lamb waves *J. Appl. Phys.* **115** 204513

[45] Joshi S G and Jin Y 1991 Excitation of ultrasonic Lamb waves in piezoelectric plates *J. Appl. Phys.* **69** 8018–24

[46] Joshi S G and Jin Y 1991 Propagation of ultrasonic Lamb waves in piezoelectric plates *J. Appl. Phys.* **70** 4113–20

[47] Zhou J, Pang H F, Garcia-Gancedo L, Iborra E, Clement M, De Miguel-Ramos M, Jin H, Luo J K, Smith S, Dong S R, Wang D M and Fu Y Q 2015 Discrete microfluidics based on

aluminum nitride surface acoustic wave devices *Microfluid. Nanofluidics* **18** 537–48

[48] Erturk A A and Inmann D J 2011 *Piezoelectric Energy Harvesting* (John Wiley and Sons)

Figure list

Fig. 1. Resonant frequencies as a function of wavelength of ZnO/Al foil devices with wavelengths in range of 20-800 μm; with both theoretical and measurement data showing good agreements.

Fig. 2. FEA simulation of vibration modes for ZnO/Al foil based SAW devices. Thicknesses of Al foil and ZnO are set to be 50 μm and 5 μm, respectively. The wavelength of SAW devices varies from 12 to 800 μm.

Fig. 3 (a) FEA simulation of hybrid modes for ZnO/Al foil based SAW devices. Thicknesses of Al foil and ZnO are set to be 50 μm and 5 μm, respectively. The wavelength of SAW devices varies from 36 to 80 μm. (b) Displacement ratio between the backside and the top side of the device showing a clear transition zone between R0 and A0 modes.

Fig. 4. Experimentally measured reflection spectra (S_{11}) of various modes for the ZnO/Al foil SAW devices; (a) for larger wavelength range (64-200 μm); and (b) for smaller wavelength range (20-32 μm). (c) The simulated and measured resonant frequency of the devices as a function of wavelength (20 to 800 μm).

Fig. 5. Resonant frequency and phase velocity as a function of the thickness of ZnO piezoelectric layer when the Al foil substrate thickness is set to 50 μm, the wavelength is set to be (a) 12 μm; (b) 64 μm; (c) 400 μm.

Fig. 6. Resonant frequency and phase velocity as a function of Al thickness. ZnO is 5 μm thick. Wavelength is set to be (a) 12 μm; (b) 64 μm; (c) 400 μm.

Fig. 7. (a) Numerical simulation of vibration modes for ZnO (5 μm)/Al(200 μm) based SAW devices. The wavelength of SAW device is varied from 100 μm to 400 μm. (b) The measured S_{11} of the devices with different wavelengths. (c) The simulated and measured resonant frequencies of different types of wave modes depend on the wavelengths of the SAW devices fabricated on Al plates with thickness of 200 μm.

Fig. 8. (a) FEA simulation of vibration modes for ZnO (5 μm)/Al(600 μm) based SAW devices. The wavelength of SAW devices is varied from 100 μm to 300 μm. (b) The simulated and measured resonant frequencies of different types of wave modes depend on the wavelengths of the SAW devices fabricated on Al plates with a thickness of 600 μm.

Highlights

- Evolution, hybridization and decoupling of multiple acoustic wave modes are investigated using finite element analysis and experimental methods
- Symmetrical and asymmetrical Lamb waves, Rayleigh waves and higher harmonic/Sezawa wave modes) are generated using thin film acoustic wave devices
- Ratios between device wavelength and substrate/film thickness are identified to be the dominant parameter in determining evolution and hybridization of multiple wave modes
- Design methodology are applicable for both sensing and microfluidic applications using flexible and bendable acoustic wave devices

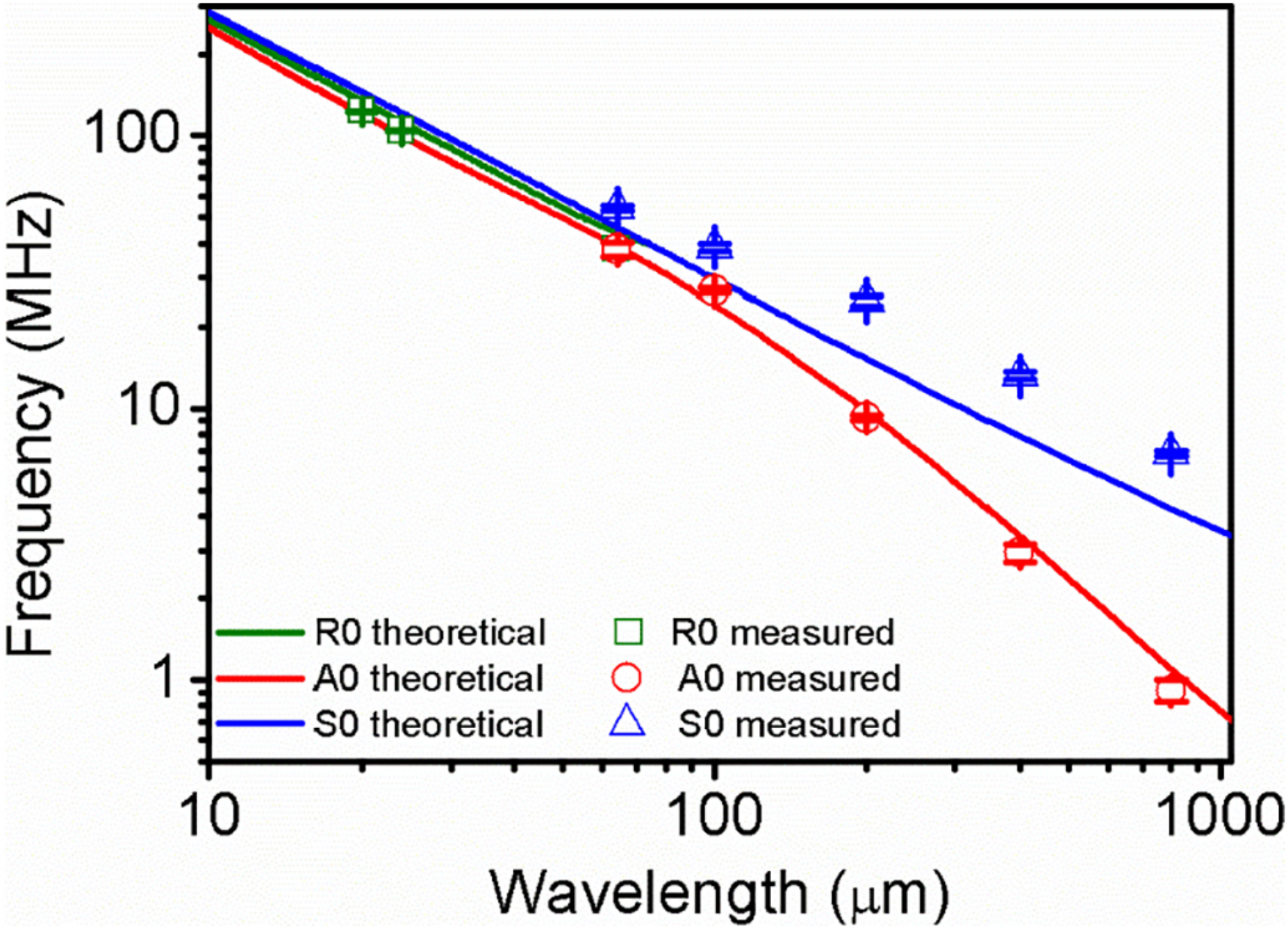
Frequency (MHz)
100
10
1
10
100
1000
Wavelength (μm)
R0 theoretical
A0 theoretical
S0 theoretical
R0 measured
A0 measured
S0 measured

Figure 1

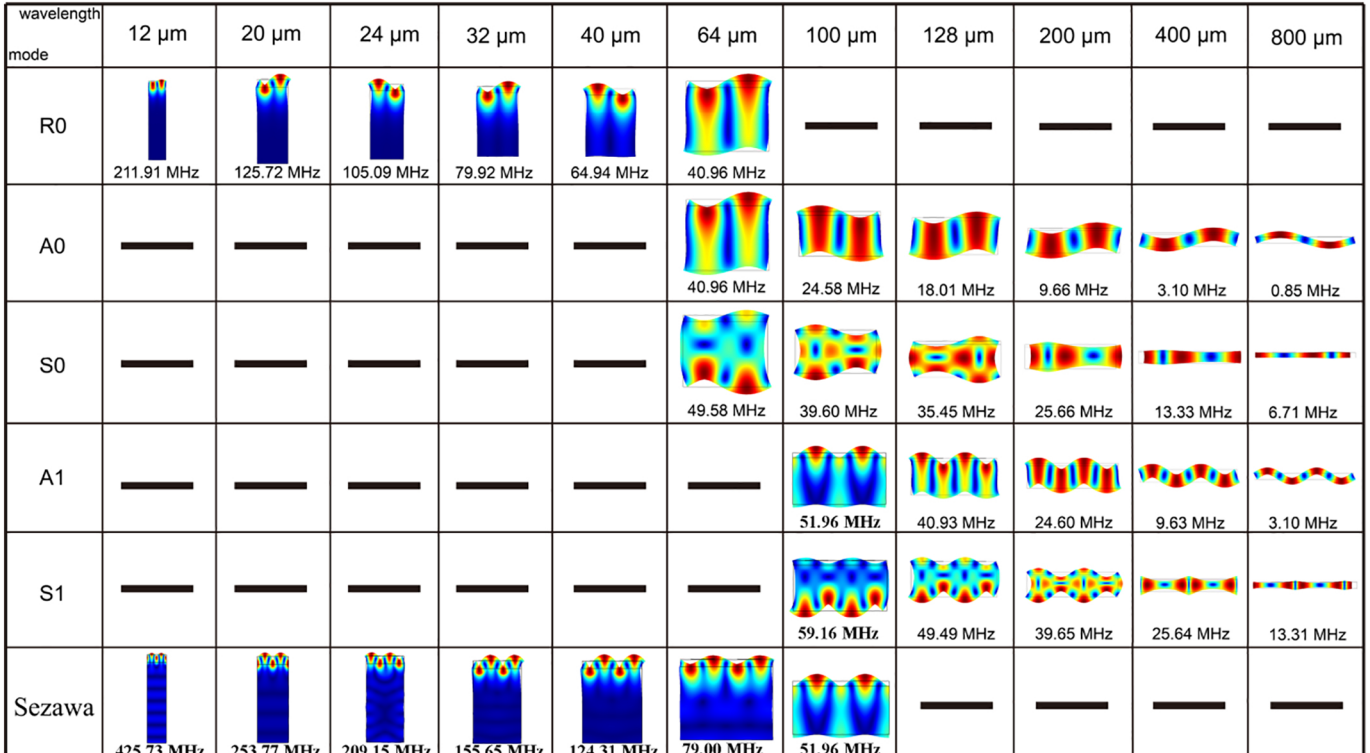
wavelength
mode
12 μm
20 μm
24 μm
32 μm
40 μm
64 μm
100 μm
128 μm
200 μm
400 μm
800 μm
R0
211.91 MHz
125.72 MHz
105.09 MHz
79.92 MHz
64.94 MHz
40.96 MHz
A0
40.96 MHz
24.58 MHz
18.01 MHz
9.66 MHz
3.10 MHz
0.85 MHz
S0
49.58 MHz
39.60 MHz
35.45 MHz
25.66 MHz
13.33 MHz
6.71 MHz
A1
51.96 MHz
40.93 MHz
24.60 MHz
9.63 MHz
3.10 MHz
S1
59.16 MHz
49.49 MHz
39.65 MHz
25.64 MHz
13.31 MHz
Sezawa
425.73 MHz
253.77 MHz
209.15 MHz
155.65 MHz
124.31 MHz
79.00 MHz
51.96 MHz

Figure 2

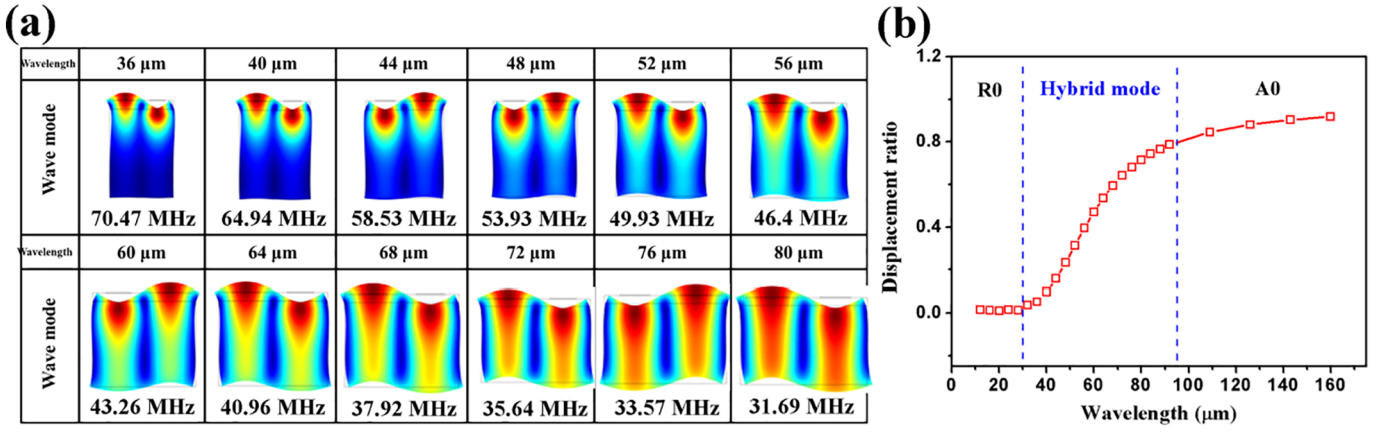
(a)
Wavelength
36 μm
40 μm
44 μm
48 μm
52 μm
56 μm
Wave mode
70.47 MHz
64.94 MHz
58.53 MHz
53.93 MHz
49.93 MHz
46.4 MHz
Wavelength
60 μm
64 μm
68 μm
72 μm
76 μm
80 μm
Wave mode
43.26 MHz
40.96 MHz
37.92 MHz
35.64 MHz
33.57 MHz
31.69 MHz
(b)
R0
Hybrid mode
A0
Displacement ratio
1.2
0.8
0.4
0.0
0
20
40
60
80
100
120
140
160
Wavelength (μm)

Figure 3

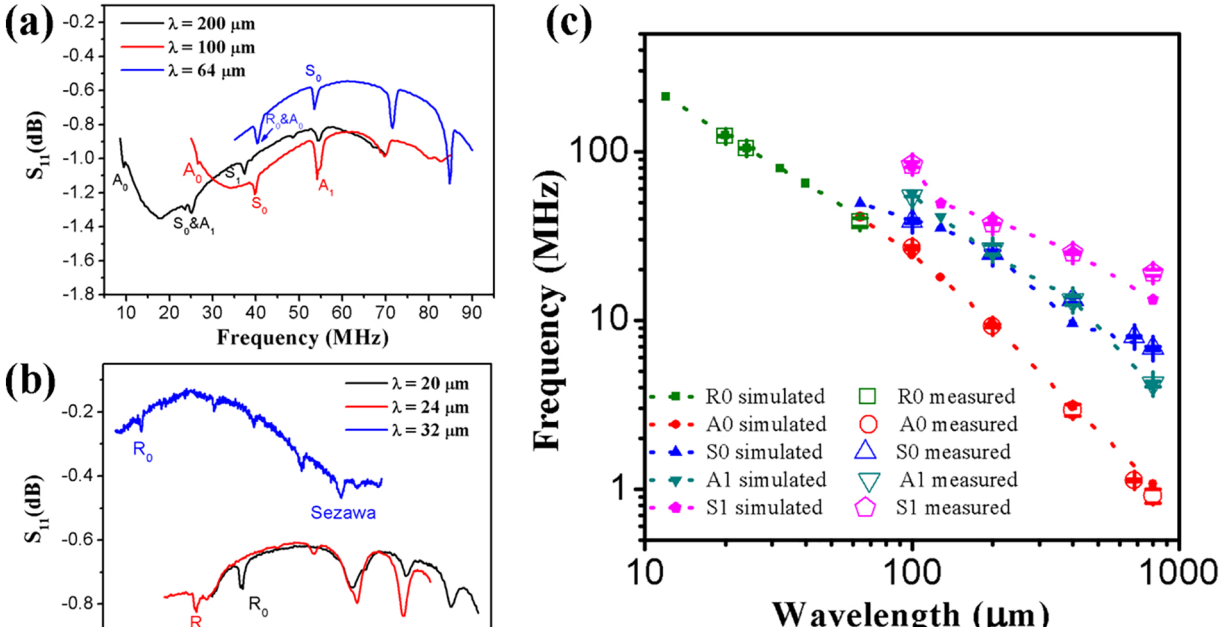
(a)
λ = 200 μm
λ = 100 μm
λ = 64 μm
S11(dB)
Frequency (MHz)
A0
S0
A1
S1
R0&A0
S0&A1
(b)
λ = 20 μm
λ = 24 μm
λ = 32 μm
R0
Sezawa
S11(dB)
Frequency (MHz)
(c)
Frequency (MHz)
Wavelength (μm)
R0 simulated
A0 simulated
S0 simulated
A1 simulated
S1 simulated
R0 measured
A0 measured
S0 measured
A1 measured
S1 measured

Figure 4

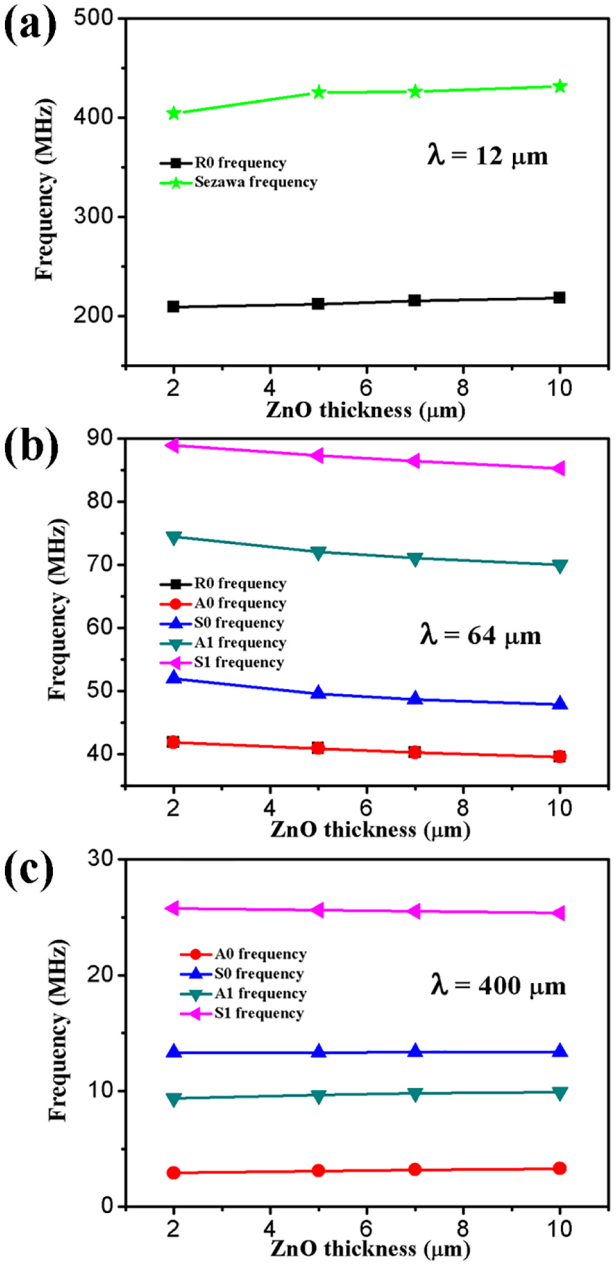
(a)
Frequency (MHz)
500
400
300
200
R0 frequency
Sezawa frequency
λ = 12 μm
2
4
6
8
10
ZnO thickness (μm)
(b)
Frequency (MHz)
90
80
70
60
50
40
R0 frequency
A0 frequency
S0 frequency
A1 frequency
S1 frequency
λ = 64 μm
2
4
6
8
10
ZnO thickness (μm)
(c)
Frequency (MHz)
30
20
10
0
A0 frequency
S0 frequency
A1 frequency
S1 frequency
λ = 400 μm
2
4
6
8
10
ZnO thickness (μm)

Figure 5

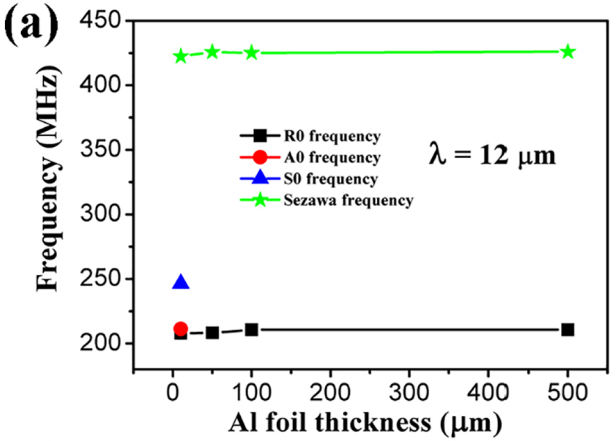
(a)
Frequency (MHz)
Al foil thickness (μm)
R0 frequency
A0 frequency
S0 frequency
Sezawa frequency
λ = 12 μm

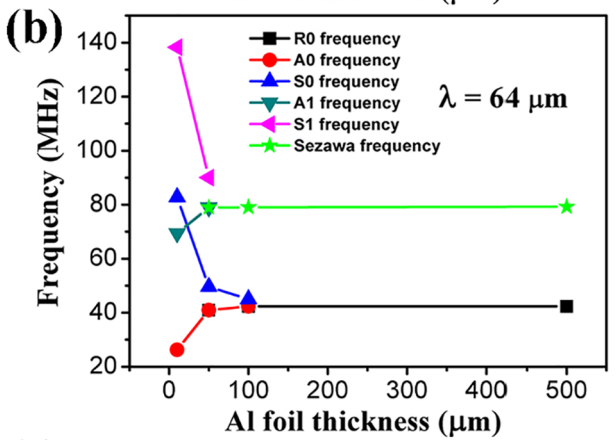
(b)
Frequency (MHz)
Al foil thickness (μm)
R0 frequency
A0 frequency
S0 frequency
A1 frequency
S1 frequency
Sezawa frequency
λ = 64 μm

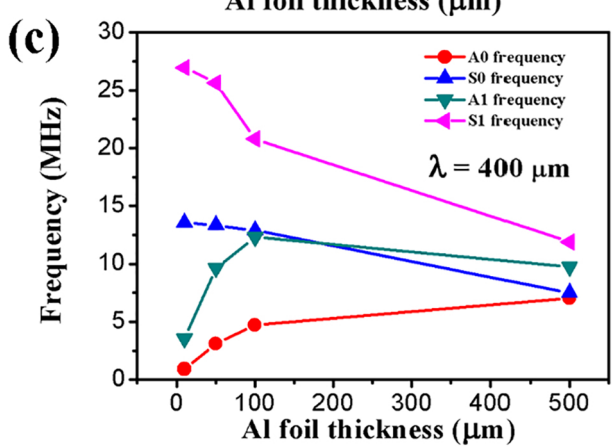
(c)
Frequency (MHz)
Al foil thickness (μm)
A0 frequency
S0 frequency
A1 frequency
S1 frequency
λ = 400 μm

Figure 6

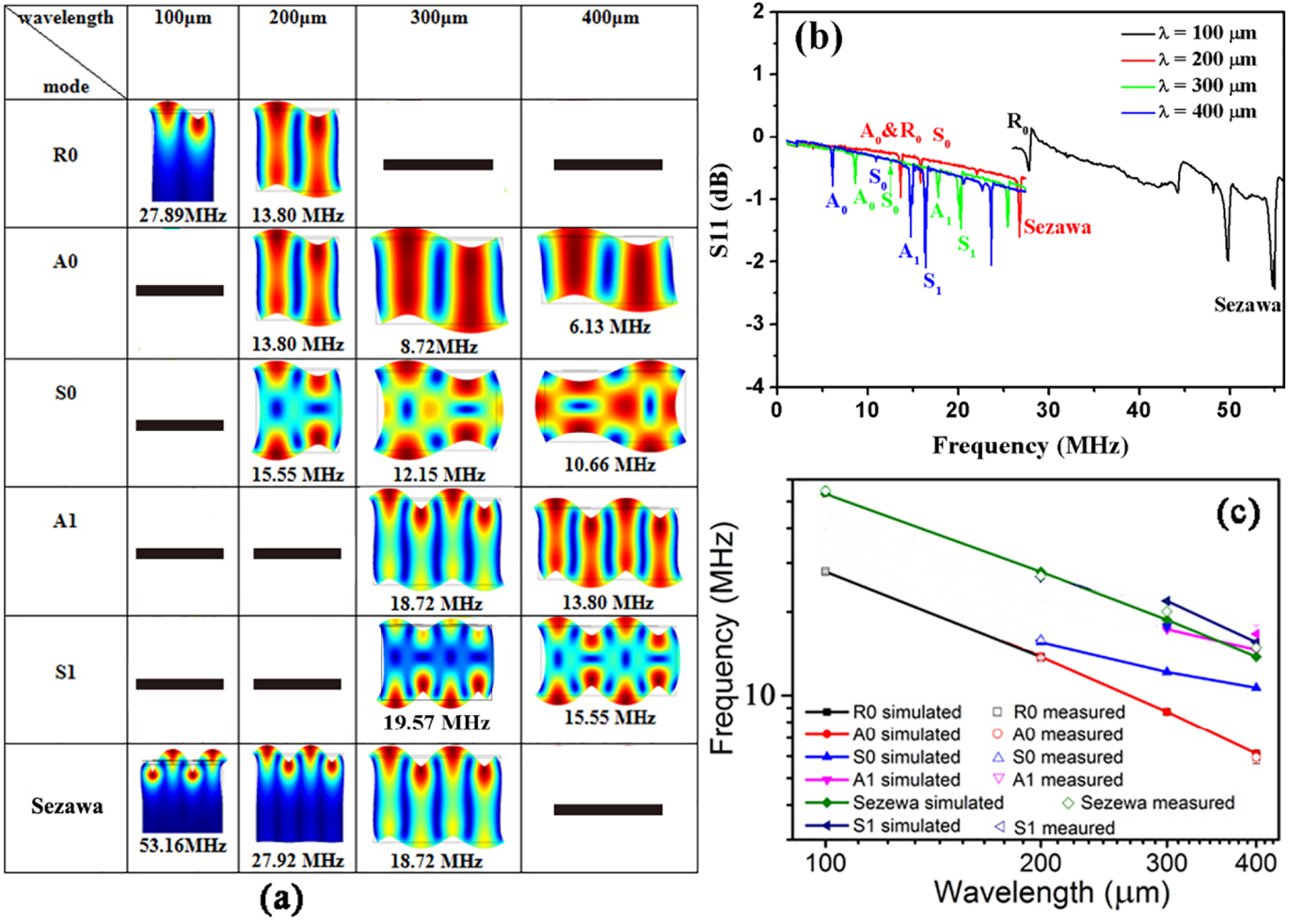
wavelength
mode
100μm
200μm
300μm
400μm
R0
27.89MHz
13.80 MHz
A0
13.80 MHz
8.72MHz
6.13 MHz
S0
15.55 MHz
12.15 MHz
10.66 MHz
A1
18.72 MHz
13.80 MHz
S1
19.57 MHz
15.55 MHz
Sezawa
53.16MHz
27.92 MHz
18.72 MHz
(a)
(b)
λ = 100 μm
λ = 200 μm
λ = 300 μm
λ = 400 μm
A0&R0 S0
R0
S0
A0 A0 S0
A1
S1
A1
S1
Sezawa
Sezawa
S11 (dB)
Frequency (MHz)
(c)
Frequency (MHz)
R0 simulated
R0 measured
A0 simulated
A0 measured
S0 simulated
S0 measured
A1 simulated
A1 measured
Sezewa simulated
Sezewa measured
S1 simulated
S1 meaured
Wavelength (μm)

Figure 7

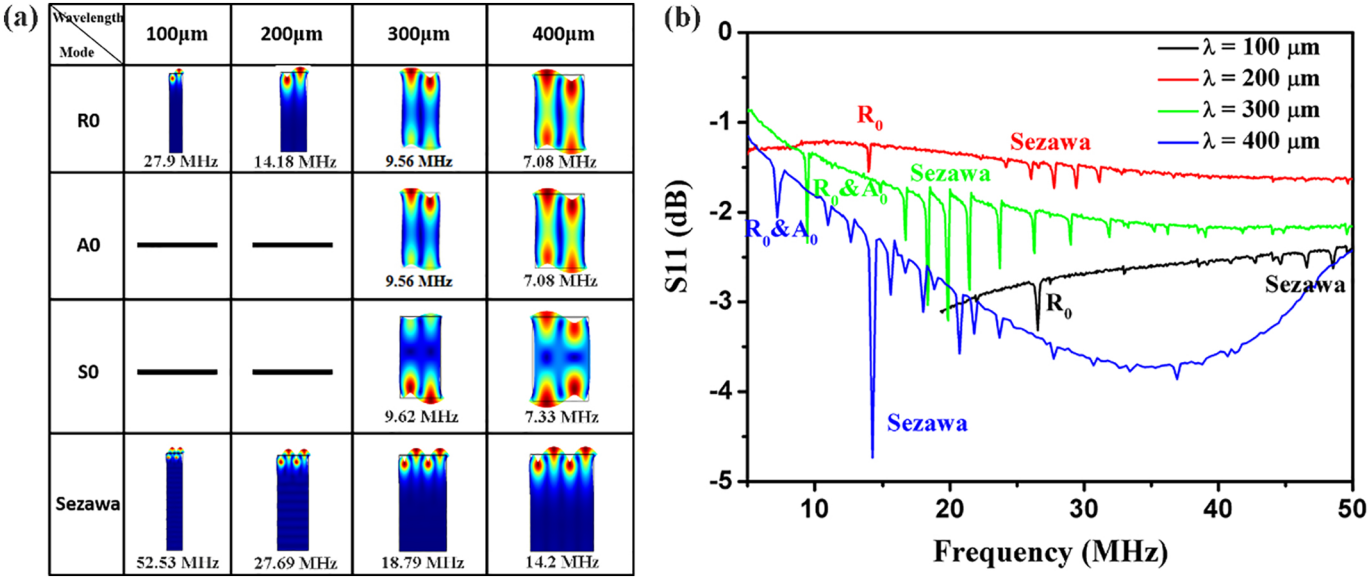
(a)
Wavelength
Mode
100μm
200μm
300μm
400μm
R0
27.9 MHz
14.18 MHz
9.56 MHz
7.08 MHz
A0
9.56 MHz
7.08 MHz
S0
9.62 MHz
7.33 MHz
Sezawa
52.53 MHz
27.69 MHz
18.79 MHz
14.2 MHz
(b)
λ = 100 μm
λ = 200 μm
λ = 300 μm
λ = 400 μm
R0
Sezawa
R0&A0
Sezawa
R0&A0
R0
Sezawa
Sezawa
S11 (dB)
Frequency (MHz)
0
-1
-2
-3
-4
-5
10
20
30
40
50

Figure 8